physica status solidi pss rrl
www.pss-rapid.com

# Ultrahigh Carrier Mobility in $Cd_3As_2$ Nanowires

*Angadjit Singh,* Piet Schoenherr, Crispin Barnes, and Thorsten Hesjedal**

**Magnetotransport measurements are carried out on nanowires of the Dirac semimetal $Cd_3As_2$. Weak antilocalization is observed at 1.9 K, consistent with the presence of strong spin–orbit interaction. With decreasing temperature, Shubnikov–de Haas oscillations are seen, revealing an ultrahigh mobility of $\approx$57 000 $cm^2 V^{-1} s^{-1}$ at 1.9 K. The strong oscillations display a linear dependence of the Landau-level index on the inverse of the magnetic field, yielding an intercept that is consistent with a $\pi$ Berry phase—the signature feature of Dirac fermions. By studying the fundamental properties of Dirac materials, new avenues can be explored by exploiting their unique properties for spintronics and magnetoelectronic devices.**

## 1. Introduction

Dirac semimetals (DSMs) are quantum materials in which the conduction and valence bands touch each other at distinct points in momentum space, known as Dirac points (DPs). Like in topological insulators, where the linear dispersion along the directions near the DP is protected by time reversal symmetry,[1] in DSMs, the linear dispersions in three directions near the DP are protected by rotational crystalline symmetry.[2–4] In DSMs, if the symmetry is broken, the DP may split into a pair of nodes, known as Weyl nodes, resulting in a Weyl semimetal.[2,3,5] In each of these pairs, the two Weyl nodes exhibit reverse chirality and monopole/antimonopole pairs with a Berry curvature to ensure a net zero flux.[6,7] This is particularly advantageous as it can host topologically protected massless conducting surface states.[8] The exploitation of these exotic properties has paved the way for topological physics and demonstrated, for example, the quantum Hall effect,[9] the quantized anomalous Hall effect,[10] the quantized photocurrent effect,[11,12] giant magnetoresistance (MR),[13] and Floquet–Bloch[14] states to name a few. One such material in the family of DSMs is $Cd_3As_2$, which has a pair of DPs distributed equally away from the $\Gamma$ point along the [001]-direction at $\pm k_D$ in the Brillouin zone, confirmed using ARPES where a linear dispersion near the DPs was observed.[15,16] Bulk $Cd_3As_2$ as well as nanomaterials also demonstrate ultrahigh carrier mobility[17–19] in transport measurements, Landau quantization,[20] Shubnikov–de Haas oscillations,[9,21–23] and very large linear positive and negative MR values[24,25] depending on the measurements geometry. The unique band structure of DSMs can also give rise to many other topological phases such as topological superconductors.[26] To make things more advantageous for devices, its Fermi surface is also very close to the DPs. $Cd_3As_2$ nanowires have been shown to exhibit universal conductance fluctuations,[13,22,27,28] phase-shifted Aharonov–Bohm (AB) oscillations,[28] as well as suppressed Klein tunneling in quantum dot-hosting nanowires.[29] $Cd_3As_2$ nanowires also have intriguing photoconductance properties, e.g., a large photoresponsivity[30] and helicity-dependent THz emission. By performing THz emission spectroscopy on a nanowire ensemble, both broadband (few cycle) and narrowband (multicycle) THz pulses were generated upon near-infrared photoexcitation by switching the polarization of light from linear to circular polarization, respectively.[31,32] Note that our nanowires crystallize in the noncentrosymmetric space group $I4_1cd$, while bulk $Cd_3As_2$ has tetragonal crystal structure belonging to the centrosymmetric $I4_1/acd$ space group. In a recent work by Park et al., it was further demonstrated that metastable nanowires in the tetragonal $P4_2/nbc$ and $P4_2/nmc$ phases can be stabilized by varying the deposition temperature.[30] Considering the promising THz properties of $Cd_3As_2$, it is important to investigate the electrical transport properties of $Cd_3As_2$ nanowires in the stable $I4_1cd$ phase.[33]

In this work, using electrical transport on $Cd_3As_2$ nanowires, we demonstrate the weak antilocalization effect consistent with strong spin–orbit interactions followed by an ultrahigh mobility characteristic of a perfect $\pi$ Berry phase evidencing Dirac fermion-like Shubnikov–de-Haas (SdH) oscillations.

## 2. Results and Discussion

The $Cd_3As_2$ nanowires were grown by chemical vapor deposition and transferred onto an electrode array for magnetotransport measurements (**Figure 1**) in an Oxford Instruments cryostat with a base temperature of 1.9 K. **Figure 2**a shows the resistance of the device with respect to temperature with zero field cooling (0 T)

A. Singh, P. Schoenherr, T. Hesjedal
Clarendon Laboratory
Department of Physics
University of Oxford
Oxford OX1 3PU, UK
E-mail: angadjit.singh@physics.ox.ac.UK;
thorsten.hesjedal@physics.ox.ac.UK

C. Barnes
Cavendish Laboratory
Department of Physics
University of Cambridge
Cambridge CB3 0HE, UK

The ORCID identification number(s) for the author(s) of this article can be found under https://doi.org/10.1002/pssr.202200365.



**DOI: 10.1002/pssr.202200365**

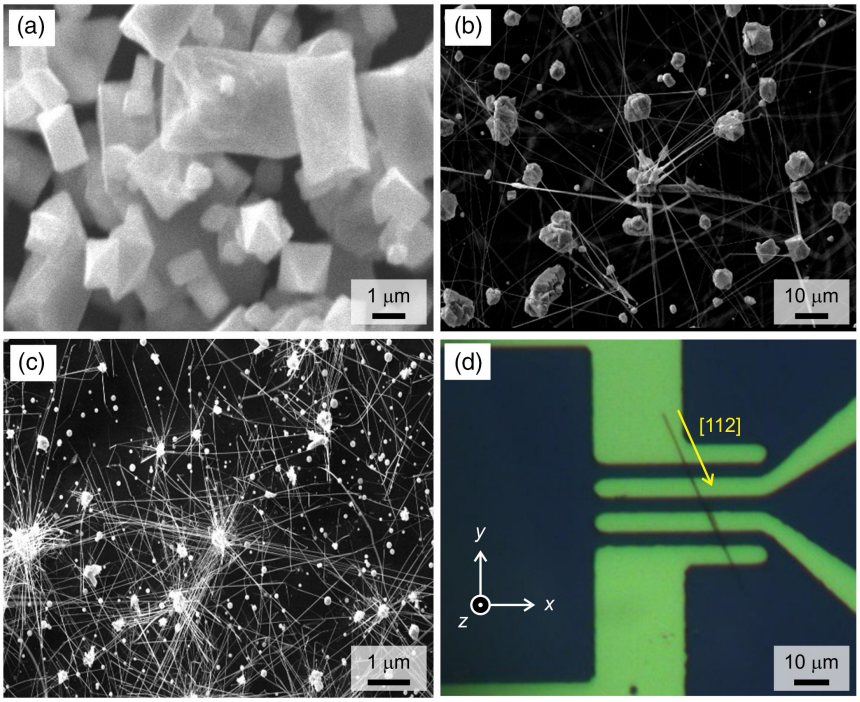


**Figure 1.** SEM micrographs of as-grown $Cd_3As_2$ samples as a function of carrier gas flow. a) Microcrystal growth of $Cd_3As_2$ (300 sccm), b) mixed cluster and nanowire growth (100 sccm), and c) nanowire growth from clusters forming a mesh network (25 sccm). d) A nanowire (taken from the sample in (c)) placed across microlithographically defined electrodes. The growth direction of the nanowire was along the [112]-direction (as indicated by the yellow arrow).

and field cooling (0.25 T). Both curves show a semiconductor-like behavior as the temperature is reduced (resistance increasing with decreasing temperature), similar to other DSMs, such as $Na_3Bi$ and $ZrTe_5$, attributed to a low carrier density.[34,35] The zero-field cooled curve shows a metallic response close to ≈50 K which then flattens out below 20 K, while the field cooling result does not show any signs of a metallic behavior. As semimetals are gapless, carriers in the valence band may be deactivated thermally if the Fermi level is close to the DP as the temperature goes down. But, below a critical temperature of ≈50 K, the thermal energy is low enough to activate carriers to the conduction band above the Fermi level giving rise to the metallic response. A far as we know, this metallic response differs significantly from bulk $Cd_3As_2$ crystals. These have a very high carrier concentration and their Fermi level lies far above the DP.[17,20] Distinctively, our wires have a very low carrier density (discussed later in the Results section), which implies that the Fermi level is close to the DP. The activation energy can also be deduced by fitting the high-temperature resistance to the equation $R_{xx} \sim \exp(E_a/k_B T)$, where $E_a$ is the activation energy (inset of Figure 2a). $E_a$ was extracted to be ≈20 meV.

Figure 2b displays the longitudinal resistance $R_{xx}$ as a function of magnetic field at 1.9 K, applied perpendicular to the longitudinal axis of the nanowire. Quantum oscillations are clearly visible with an obtuse dip feature at zero field, corresponding to weak antilocalization (WAL).[12,36] WAL occurs in systems with strong spin–orbit interaction, and it is pointing toward the existence of topologically protected surface states in $Cd_3As_2$.[28] This is also consistent with the metallic response observed in the $R_{xx}$ vs. $T$ plot in Figure 2a. To further understand the quantum oscillations, a temperature-dependent magnetic field sweep was performed on $R_{xx}$.

At higher fields, the MR starts to oscillate periodically giving rise to pronounced SdH fluctuations up to 50 K after which they disappear as shown in **Figure 3**a. Most researchers have observed a negative MR in DSMs and Weyl semimetals, which is believed to originate from the chiral anomaly induced charge pumping effect.[27] Here, in contrast, we observe a positive MR expected for hopping conduction, in agreement with Li et al.[25] for the magnetic field applied perpendicular to the substrate surface. As the applied magnetic field contracts the overlap of the localized state wave functions, it results in an increase of the average hopping length resulting in an increase in resistance with field.[37] A linear background was then subtracted from these graphs, and the plots of oscillation amplitude $\Delta R_{xx}$ versus $1/B$ from 1.9 to 50 K were obtained as depicted in Figure 3b. The oscillations became stronger with the increase in $B$ and decrease of $T$.

A Landau fan diagram for 1.9 K was plotted by taking the maximum and minimum of the oscillation amplitude as the half-integer and integer levels, respectively, as shown in **Figure 4**a. According to the Lifshitz–Onsager rule, it is well known that in the SdH oscillations, the Landau-level index $n$ is related to the cross-sectional area of the Fermi surface $S_F$ via $2\pi(n+\gamma) = S_F\hbar/eB$, where $\gamma$ is the Berry phase. The linear extrapolation of the Landau-level index plot to $1/B = 0$ yields an intercept of −0.129, which is close to the value of 1/8 expected for a Dirac system with a Berry phase of $\pi$.[38] This is strong evidence

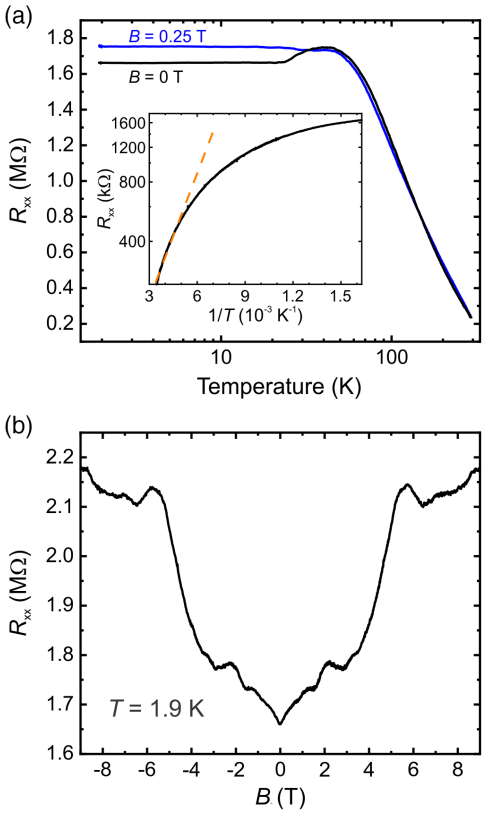


**Figure 2.** a) Resistance $R_{xx}$ vs temperature measured at 0 and 0.25 T. The semiconducting-like $R$-$T$ behavior shows that the Fermi level may be close to the Dirac point. The thermal movement of charges can increase the conductance resulting in a resistance increase with decreasing temperature. The inset shows the activation energy acquired by fitting the high-temperature resistance to the equation $R_{xx} \sim \exp(E_a/k_BT)$, where $E_a$ is the activation energy. $E_a$ was extracted to be ≈20 meV. b) Resistance $R_{xx}$ vs field $B$ at a temperature of 1.9 K, showing quantum oscillations.

for Dirac fermion transport in $Cd_3As_2$ nanowires.[28] As demonstrated by Wang et al.,[28] on applying an external magnetic field, time reversal symmetry is broken that splits the DPs into two pairs of Weyl nodes. The chirality of these nontrivial surface states is nondegenerate. The lifting of the degeneracy results in an additional Berry phase $\pi$ for electrons on cyclotron orbits.

The observation of SdH oscillations can also be used to calculate parameters of the carrier transport. To find the oscillation frequency $B_F$, a fast Fourier transform (FFT) was performed on the SdH oscillations giving a value of 3.16 T as shown in the inset of Figure 3b. By using the equation $B_F = (\phi_0/2\pi^2)S_F$, where $\phi_0 = h/2e$, a Fermi surface of $S_F = 0.33 \times 10^{-3}$ Å$^{-2}$ was determined. Here, if we assume that the Fermi surface is circular, i.e., a Dirac-type band dispersion, the relations $S_F = \pi k_F^2$ (Fermi wave vector $k_F$) and $n_{3D} = k_F^3/(3\pi^2)$ (3D carrier density) are valid.[17] In this way, $k_F$ was estimated to be 0.0097 Å$^{-1}$ and $n_{3D} = 3 \times 10^{16}$ cm$^{-3}$. This value of $n_{3D}$ is much smaller than in bulk $Cd_3As_2$, meaning that the Fermi level is very close to the DP.[25]

To analyze the characteristics of transport further, the cyclotron mass ($m_{cyc}$) was calculated. The temperature-dependent SdH oscillation amplitude $\Delta R_{xx}$ was first extracted by following the Lifshitz–Kosevich (LK) theory given by $\Delta R_{xx}(T)/R_{xx}(0) = \lambda(T)/\sinh(\lambda(T))$, where the thermal factor is given by $\lambda(T) = 2\pi^2 k_b T m_c/\hbar eB$, and with $m_{cyc} = E_F/v_F^2$ the effective cyclotron mass. As shown in Figure 4b, the best fit gives a cyclotron mass of $m_{cyc} = 0.053m_e$. The Fermi velocity $v_F = \hbar k_F/m_{cyc}$ and energy $E_F = m_{cyc}v_F^2$ can be calculated as 2.12 m s$^{-1}$ and 13.5 meV, respectively. Moreover, from a Dingle plot,[39] the quantum lifetime $\tau$ time can be calculated from the Dingle factor $e^{-D}$, where $D = 2\pi^2 E_F/\tau eBv_F^2$. Since $\Delta R_{xx}(T)/\Delta R_{xx}(0)$ is proportional to $e^{-D}\lambda(T)/\sinh(\lambda(T))$, the quantum lifetime $\tau$ can be found from the slope of the logarithmic plot of $[\Delta R_{xx}(T)/\Delta R_{xx}(0)]B\sinh(\lambda)$ vs $1/B$. By using the cyclotron mass, the quantum lifetime $\tau$ was estimated to be $1.73 \times 10^{-12}$ s. Other important parameters such as mean free path $l = v_F\tau$ and the mobility $\mu_{SdH}$ were calculated and summarized in **Table 1** and **2**. This means that the mobility of our $Cd_3As_2$ nanowires is among the highest reported in the literature.[18,22,27]

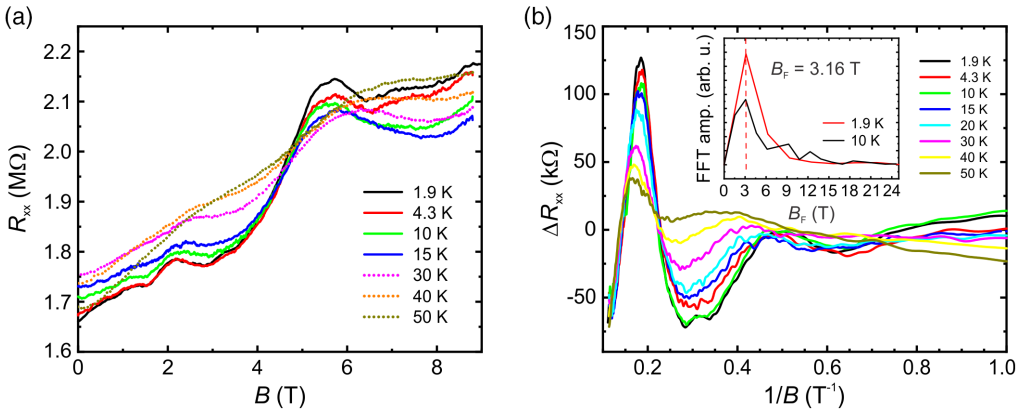


**Figure 3.** a) Plot of resistance $R$ vs magnetic field $B$ at various temperatures from 1.9 to 50 K showing SdH oscillations. b) Oscillating part of $\Delta R_{xx}$ as a function of $B$. The inset shows the fast Fourier transform (FFT) on the SdH oscillations with a peak at 3.16 T.

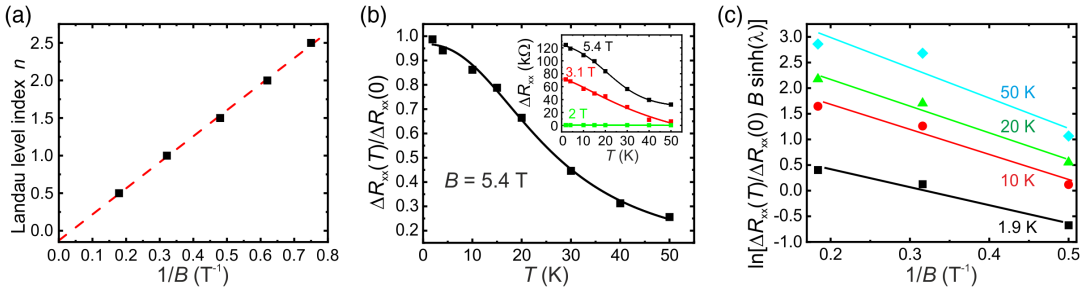


**Figure 4.** a) Landau fan diagram, i.e., plot of the Landau-level index $n$ vs $1/B$, obtained from the LK analysis of the SdH oscillations. The linear fit to the data gives an intercept at −0.129 (for $1/B$=0). The value for $\beta$ extracted in this way is close to 1/8, representative of a 3D Dirac fermion system with a Berry phase of $\pi$. b) Normalized resistance amplitude $\Delta R_{xx}(T)/\Delta R_{xx}(0)$ vs. temperature at 5.4 T. The inset shows $\Delta R_{xx}$ as a function of temperature at different fields from which the effective mass, $m_{cyc}$, can be determined. c) Dingle plot allowing for the extraction of the quantum lifetime $\tau$ and mobility $\mu_{SdH}$.

**Table 1.** Calculated electrical parameters at 1.9 K.

| $B_F$ [T] | $S_F$ [Å$^{-2}$] | $k_F$ [Å$^{-1}$] | $\nu_F$ [$10^5$ m/s] | $E_F$ [meV] | $l$ [nm] | $m_{cyc}$ [$m_e$] | $\tau$ [$10^{-12}$ s] |
|---|---|---|---|---|---|---|---|
| 3.16 | 0.33 | 0.0097 | 2.12 | 13.5 | 366 | 0.053 | 1.73 |

**Table 2.** Mobility for $Cd_3As_2$ calculated at different temperatures.

| $T$ [K] | 1.9 | 4 | 10 | 20 | 50 |
|---|---|---|---|---|---|
| $\mu_{SdH}$ [cm$^{-2}$ V$^{-1}$ s$^{-1}$] | 56 884 | 40 129 | 36 386 | 37 897 | 33 599 |

## 3. Summary and Conclusion

In summary, $Cd_3As_2$ were processed into four-point probe devices using photolithography and electrical measurements were carried out on them. The results display a semiconductor-like behavior with a clear metallic response at low temperatures consistent with the presence of topological surface states. Weak antilocalization was observed that confirms strong spin–orbit coupling in the material system. Clear SdH oscillations were visible at low temperatures from 1.9 to 50 K. The analysis of the oscillations reveals various electrical transport parameters with an ultrahigh mobility at 1.9 K corresponding to 56 884 cm$^2$ V$^{-1}$ s$^{-1}$. The results shed light to understand the fundamental properties of nanowires that are very important to push the material system toward versatile and practical device applications.

## 4. Experimental Section

*Sample Preparation*: $Cd_3As_2$ nanowires were grown using chemical vapor deposition on Si(100) substrates employing a self-catalyzed process. A precursor of $Cd_3As_2$ powder was placed in a horizontal tube furnace at 750 °C. Several Si(100) substrates were placed in a quartz boat, which was kept downstream where the (thermocouple) temperature was ≈200 °C. By adjusting the flow rate of the $N_2$ carrier gas, the structural properties of the as-grown material can be tuned. For a high $N_2$ flow rate of 300 sccm, microclusters were formed as shown in Figure 1a. In contrast, for a lower flow rate (100 sccm), nanowires and clusters form (Figure 1b), while nanowires with a diameter of several 10 nm dominate at 25 sccm (Figure 1c). These $\alpha$-$Cd_3As_2$ nanowires crystallize in the noncentrosymmetric space group $I4_1cd$.

More details on the structural properties of the nanostructures (X-ray diffraction and transmission electron microscopy), their composition (energy-dispersive X-ray spectroscopy), and Raman spectroscopy can be found in Ref. [33]. Note that we will call our nanoscale structures investigated here nanowires to be consistent with previous publications; however, they could also be classified as nanoribbons.[33]

*Device Fabrication*: After growth, the nanowires were carefully harvested from the Si(100) substrate and randomly dispersed on top of a new, clean $Si/SiO_2$ (300 nm) substrate using microtools. Next, an isolated wire was located in an optical microscope, and micrometer-sized electrodes were defined using standard photolithography techniques. The distance between each electrode was 5 µm. In order to form ohmic contacts between the nanowire and the electrodes, 20/80 nm of Ti/Au was deposited after a quick $Ar^+$ etching treatment in vacuum. The sample was then placed in a lead-less chip carrier (LCC), followed by Au wire bonding.

*Electrical Characterization*: The LCC was mounted inside a sample holder and inserted into an Oxford Instruments cryostat with a base temperature of 1.9 K. For the measurements presented in the manuscript, the magnetic field was applied normal to the substrate plane ($B||z$; see Figure 1d). Standard AC electrical four-terminal measurements were carried out employing a Stanford SR830 lock-in amplifier at a frequency of 77 Hz using a constant current of 100 nA.

## Acknowledgements

A.S. and T.H. acknowledge funding from the Leverhulme Trust (RPG-2020-358). This research utilized equipment funded by the John Fell Oxford University Press Research Fund. P.S. acknowledges partial funding by EPSRC and Corpus Christi College (University of Oxford). The authors also thank RCaH for access to the SEM/EDS facility.

## Conflict of Interest

The authors declare no conflict of interest.

## Data Availability Statement

The data that support the findings of this study are available from the corresponding author upon reasonable request.

## Keywords

$Cd_3As_2$, Dirac semimetals, electrical transport, Weyl semimetals

Received: September 23, 2022
Revised: October 23, 2022
Published online:

[1] M. Z. Hasan, C. L. Kane, *Rev. Mod. Phys.* **2010**, *82*, 3045.
[2] X. Wan, A. M. Turner, A. Vishwanath, S. Y. Savrasov, *Phys. Rev. B* **2011**, *83*, 205101.
[3] A. A. Burkov, L. Balents, *Phys. Rev. Lett.* **2011**, *107*, 127205.
[4] B. J. Yang, N. Nagaosa, *Nat. Commun.* **2014**, *5*, 4898.
[5] K.-Y. Yang, Y.-M. Lu, Y. Ran, *Phys. Rev. B* **2011**, *84*, 075129.
[6] G. E. Volovik, in *The Universe in a Helium Droplet*, Clarendon Press, Oxford, UK, **2003**.
[7] H. Weng, C. Fang, Z. Fang, B. A. Bernevig, X. Dai, *Phys. Rev. X* **2015**, *5*, 011029.
[8] D. A. Kealhofer, M. Goyal, T. N. Pardue, S. Stemmer, *Phys. Rev. B* **2021**, *104*, 035435.
[9] C. Zhang, A. Narayan, S. Lu, J. Zhang, H. Zhang, Z. Ni, X. Yuan, Y. Liu, J.-H. Park, E. Zhang, W. Wang, S. Liu, L. Cheng, L. Pi, Z. Sheng, S. Sanvito, F. Xiu, *Nat. Commun.* **2017**, *8*, 1272.
[10] C.-Z. Chang, J. Zhang, X. Feng, J. Shen, Z. Zhang, M. Guo, K. Li, Y. Ou, P. Wei, L.-L. Wang, Z.-Q. Ji, Y. Feng, S. Ji, X. Chen, J. Jia, X. Dai, Z. Fang, S.-C. Zhang, K. He, Y. Wang, L. Lu, X.-C. Ma, Q.-K. Xue, *Science* **2013**, *340*, 167.
[11] F. de Juan, A. G. Grushin, M. Takahiro, J. E. Moore, *Nat. Commun.* **2017**, *8*, 15995.
[12] Z. Wang, H. Weng, Q. Wu, X. Dai, Z. Fang, *Phys. Rev. B* **2013**, *88*, 125427.
[13] C.-Z. Li, J.-G. Li, L.-X. Wang, L. Zhang, J.-M. Zhang, D. Yu, Z.-M. Liao, *ACS Nano* **2016**, *10*, 6020.
[14] H. Hübener, M. A. Sentef, U. D. Giovannini, A. F. Kemper, A. Rubio, *Nat. Commun.* **2017**, *8*, 13940.
[15] M. Neupane, S.-Y. Xu, R. Sankar, N. Alidoust, G. Bian, C. Liu, I. Belopolski, T.-R. Chang, H.-T. Jeng, H. Lin, A. Bansil, F. Chou, M. Z. Hasan, *Nat. Commun.* **2014**, *5*, 3786.
[16] Z. K. Liu, J. Jiang, B. Zhou, Z. J. Wang, Y. Zhang, H. M. Weng, D. Prabhakaran, S.-K. Mo, H. Peng, P. Dudin, T. Kim, M. Hoesch, Z. Fang, X. Dai, Z. X. Shen, D. L. Feng, Z. Hussain, Y. L. Chen, *Nature Mater.* **2014**, *13*, 677.
[17] T. Liang, Q. Gibson, M. N. Ali, M. Liu, R. J. Cava, N. P. Ong, *Nature Mater.* **2015**, *14*, 280.
[18] Z.-G. Chen, C. Zhang, Y. Zou, E. Zhang, L. Yang, M. Hong, F. Xiu, J. Zou, *Nano Lett.* **2015**, *15*, 5830.
[19] A. D. Rice, J. Nelson, A. G. Norman, P. Walker, K. Alberi, *ACS Appl. Electron. Mater.* **2022**, *4*, 729.
[20] S. Jeon, B. B. Zhou, A. Gyenis, B. E. Feldman, I. Kimchi, A. C. Potter, Q. D. Gibson, R. J. Cava, A. Vishwanath, A. Yazdani, *Nature Mater.* **2014**, *13*, 851.
[21] L. P. He, X. C. Hong, J. K. Dong, J. Pan, Z. Zhang, J. Zhang, S. Y. Li, *Phys. Rev. Lett.* **2014**, *113*, 246402.
[22] E. Zhang, Y. Liu, W. Wang, C. Zhang, P. Zhou, Z.-G. Chen, J. Zou, F. Xiu, *ACS Nano* **2015**, *9*, 8843.
[23] M. Uchida, Y. Nakazawa, S. Nishihaya, K. Akiba, M. Kriener, Y. Kozuka, A. Miyake, Y. Taguchi, M. Tokunaga, N. Nagaosa, Y. Tokura, M. Kawasaki, *Nat. Commun.* **2017**, *8*, 2274.
[24] A. Narayanan, M. D. Watson, S. F. Blake, N. Bruyant, L. Drigo, Y. L. Chen, D. Prabhakaran, B. Yan, C. Felser, T. Kong, P. C. Canfield, A. I. Coldea, *Phys. Rev. Lett.* **2015**, *114*, 117201.
[25] C.-Z. Li, L.-X. Wang, H. Liu, J. Wang, Z.-M. Liao, D.-P. Yu, *Nat. Commun.* **2015**, *6*, 10137.
[26] M. M. Sharma, P. Sharma, N. K. Karn, V. P. S. Awana, *Supercond. Sci. Technol.* **2022**, *35*, 083003.
[27] H. Li, H. He, H.-Z. Lu, H. Zhang, H. Liu, R. Ma, Z. Fan, S.-Q. Shen, J. Wang, *Nat. Commun.* **2016**, *7*, 10301.
[28] L.-X. Wang, C.-Z. Li, D.-P. Yu, Z.-M. Liao, *Nat. Commun.* **2016**, *7*, 10769.
[29] M. Jung, K. Yoshida, K. Park, X.-X. Zhang, C. Yesilyurt, Z. B. Siu, M. B. A. Jalil, J. Park, J. Park, N. Nagaosa, J. Seo, K. Hirakawa, *Nano Lett.* **2018**, *18*, 1863.
[30] K. Park, M. Jung, D. Kim, J. R. Bayogan, J. H. Lee, S. J. An, J. Seo, J. Seo, J.-P. Ahn, J. Park, *Nano Lett.* **2020**, *20*, 4939.
[31] J. L. Boland, C. Q. Xia, D. A. Damry, P. Schoenherr, T. Hesjedal, L. M. Herz, M. B. Johnston, in *45th Int. Conf. on Infrared, Millimeter, and Terahertz Waves (IRMMW-THz)*, Buffalo, New York, USA, 8–13 November **2020**, https://doi.org/10.1109/IRMMW-THz46771.2020.
[32] J. L. Boland, D. A. Damry, C. Q. Xia, P. Schoenherr, D. Prabhakaran, L. M. Herz, T. Hesjedal, M. B. Johnston, *ACS Nano* **2022**, Unpublished.
[33] P. Schönherr, T. Hesjedal, *Appl. Phys. Lett.* **2015**, *106*, 013115.
[34] J. Xiong, S. K. Kushwaha, T. Liang, J. W. Krizan, M. Hirschberger, W. Wang, R. J. Cava, N. P. Ong, *Science* **2015**, *350*, 413.
[35] J. Wang, Y. Jiang, T. Zhao, Z. Dun, A. L. Miettinen, X. Wu, M. Mourigal, H. Zhou, W. Pan, D. Smirnov, Z. Jiang, *Nat. Commun.* **2021**, *12*, 6758.
[36] W. Yu, D. X. Rademacher, N. R. Valdez, M. A. Rodriguez, T. M. Nenoff, W. Pan, *Nanotechnology* **2022**, *33*, 415002.
[37] I. Crassee, R. Sankar, W.-L. Lee, A. Akrap, M. Orlita, *Phys. Rev. Materials* **2018**, *2*, 120302.
[38] H. Murakawa, M. S. Bahramy, M. Tokunaga, Y. Kohama, C. Bell, Y. Kaneko, N. Nagaosa, H. Y. Hwang, Y. Tokura, *Science* **2013**, *342*, 1490.
[39] D. Shoenberg, in *Magnetic Oscillations in Metals*, Cambridge University Press, Cambridge, UK **1984**.